Journal of Materials Chemistry B

ROYAL SOCIETY OF CHEMISTRY

PAPER

View Article Online
View Journal | View Issue

Open Access Article. Published on 28 May 2024. Downloaded on 11/8/2025 11:26:02 AM. This article is licensed under a Creative Commons Attribution 3.0 Unported Licence.

Check for updates

Cite this: J. Mater. Chem. B, 2024, 12, 6500

Supramolecular red-light-photosensitized nitric oxide release with fluorescence self-reporting within biocompatible nanocarriers

Francesca Laneri,[a] Cristina Parisi,[a] Mimimorena Seggio,[a] Aurore Fraix,[a] Giuseppe Longobardi,[b] Ovidio Catanzano,[c] Fabiana Quaglia *[b] and Salvatore Sortino *[a]

Received 17th February 2024, Accepted 26th May 2024

DOI: 10.1039/d4tb00325j

rsc.li/materials-b

The strict dependence of the biological effects of nitric oxide (NO) on its concentration and generation site requires this inorganic free radical to be delivered with precise spatiotemporal control. Light-activation by suitable NO photoprecursors represents an ideal approach. Developing strategies to activate NO release using long-wavelength excitation light in the therapeutic window (650–1300 nm) is challenging. In this contribution, we demonstrate that NO release by a blue-light activatable NO photodonor (NOPD) with self-fluorescence reporting can be triggered catalytically by the much more biocompatible red light exploiting a supramolecular photosensitization process. Different red-light absorbing photosensitizers (PSs) are co-entrapped with the NOPD within different biocompatible nanocarriers such as Pluronic® micelles, microemulsions and branched cyclodextrin polymers. The intra-carrier photosensitized NO release, involving the lowest, long-lived triplet state of the PS as the key intermediate and its quenching by the NOPD, is competitive with that by molecular oxygen. This allows NO to be released with good efficacy, even under aerobic conditions. Therefore, the adopted general strategy provides a valuable tool for generating NO from an already available NOPD, otherwise activatable with the poorly biocompatible blue light, without requiring any chemical modification and using sophisticated and expensive irradiation sources.

Introduction

Nitric oxide (NO) is a small inorganic free radical that plays a multifaceted role in many physiological and pathophysiological processes[1,2] and is coming into the limelight as an unconventional therapeutic in treating severe diseases,[3,4] including cancer[5] and bacterial infections.[6] Over the last two decades, these intriguing prospects and the difficulties in handling gaseous NO have stimulated growing interest in developing NO-releasing precursors integrated into molecular and macromolecular scaffolds and functional materials that can store and deliver NO.[7–12] Due to the strict dependence of the biological effects of NO on its dose and concentration site,[13,14] the spatiotemporal control of NO release is a highly demanding requisite. Given that light can be easily manipulated in terms of energy, intensity, location, and duration, it represents a non-invasive, powerful tool to control the NO release in space and time with great accuracy. A significant arsenal of photo-activatable precursors, namely NO photodonors (NOPDs), based on organic and inorganic chromophoric motifs and activatable with UV and Vis light, have been developed in recent years.[15–20] In this arena, the generation of NO by one-photon excitation in the so-called "therapeutic window" (650–1300 nm)[21] with conventional and low-cost red or near-infrared (NIR) light sources is highly suitable for biomedical applications. This spectral region is, in fact, highly tissue-penetrating due to the negligible absorption of water and haemoglobin.[21] Therefore, achieving NOPDs activatable with one-photon red light is very challenging. Compared with NOPDs based on metal complexes, only a few examples of non-metal-based NOPDs controlled by one-photon red/NIR light have been reported. They involve different approaches based on red-light-harvesting antennae linked with *N*-nitrosoaniline appendages uncaging NO through photoinduced electron transfer,[22,23] red-light absorbing J-aggregates of nitrosated BODIPY chromophores[24] and thermolabile NO precursors which exploit the NIR-induced photothermia of plasmonic inorganic nanostructures.[25]

[a] PhotoChemLab, Department of Drug and Health Sciences, Viale Andrea Doria 6, 95125, Catania, Italy. E-mail: ssortino@unict.it
[b] Drug Delivery Laboratory, Department of Pharmacy, University of Napoli Federico II, Via Domenico Montesano 49, 80131, Napoli, Italy. E-mail: quaglia@unina.it
[c] Institute for Polymers, Composites and Biomaterials (IPCB-CNR), Via Campi Flegrei 34, I-80078, Pozzuoli (NA), Italy

 This journal is © The Royal Society of Chemistry 2024

Open Access Article. Published on 28 May 2024. Downloaded on 11/8/2025 11:26:02 AM.
This article is licensed under a Creative Commons Attribution 3.0 Unported Licence.

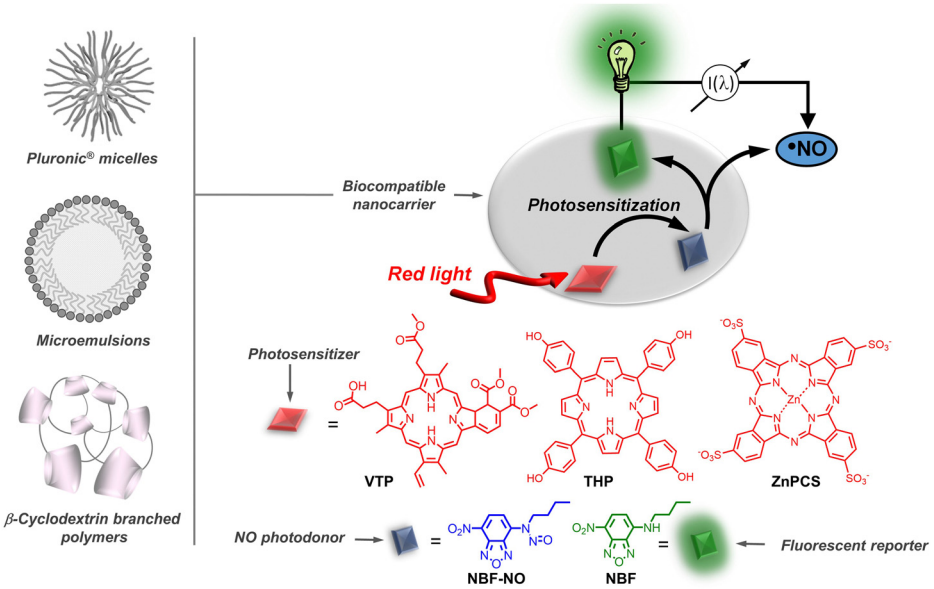

Scheme 1 Schematic of the red-light photosensitization mechanism for the NO release with fluorescent self-reporting, a sketch of the biocompatible nanocarriers structure and the molecular structures of the PSs, the NOPD and its green fluorescent reporter.

In our recent work, we have reported a straightforward approach to trigger the NO release in a catalytic fashion from **NBF-NO**,[26] a blue-light activatable NOPD[27] (Scheme 1). It involves a triplet-mediated photosensitization process upon one-photon red light excitation of verteporfin (**VTP**), a clinically approved lipophilic photosensitizer (PS) for photodynamic therapy (PDT).[28,29] A remarkable improvement of about 300 nm towards longer wavelengths was achieved without requiring any chemical modification efforts. The process occurred effectively within biodegradable polymeric nanoparticles (NPs) of methoxy-polyethyleneglycol-*b*-polycaprolactone NPs (mPEG-PCL).[26] The highly green fluorescent photoproduct NBF generated in parallel to the NO release acted as an optical NO self-reporter, permitting its easy and real-time quantification without the addition of external fluorescent probes also in the cell environment.[26]

These results prompted us to extend the applicability of the adopted strategy to different types of red-light-absorbing PSs and other biocompatible nanocarriers. The outcome is not trivial since the confinement of individual or multiple guests in the restricted environments of nanocarriers with different features can affect the photochemical processes in their nature, efficiency or both.

To this purpose, we selected, besides **VTP**, the lipophilic porphyrinoid PS **THP** (5,10,15,20-tetra(4-hydroxyphenyl)porphyrin) and the hydrophilic **ZnPCS** (Zn(II) phthalocyanine tetrasulfonate) to activate NO photorelease (Scheme 1). To promote the photosensitization reaction, we encapsulated the PS/**NBF-NO** pair in optically transparent, biocompatible nanocarriers. We tested Pluronic® micelles (PLMs) and microemulsions (MEs), both suitable to host lipophilic molecules, and a β-cyclodextrin branched polymer (poly-βCD) able to entrap both lipophilic and hydrophilic guest compounds (Scheme 1). We investigate if the communication between the excited triplet state of the PSs and the **NBF-NO** within the same hosts leads to the generation of NO and its self-fluorescent reporter. The effect of the dissolved molecular oxygen on the photosensitization reaction is also explored.

Results and discussion

Besides **VTP**, the present study was extended also to other two porphyrinoid PSs such as **THP** and **ZnPCS**, which have hydrophobic and hydrophilic features, respectively (see Scheme 1). For the sake of clarity, the absorption spectra of all the chromophoric components investigated here are shown in Fig. 1. Analogously to **VTP**, both **THP** and **ZnPCS** show typical Q-bands in the red region well beyond the absorption region of **NBF-NO** and its stable photoproduct NBF formed after NO

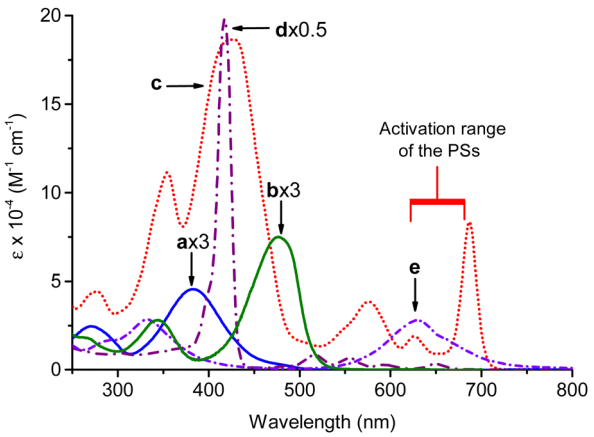

Fig. 1 Absorption spectra of **NBF-NO** (a), **NBF** (b), **VTP** (c), **THP** (d) and **ZnPCS** (e). Spectra a–d and spectrum e are recorded in MeOH and H_2O, respectively. T = 25 °C. Spectra a, b and d are multiplied for a factor, for sake of clarity.

Open Access Article. Published on 28 May 2024. Downloaded on 11/8/2025 11:26:02 AM.
This article is licensed under a Creative Commons Attribution 3.0 Unported Licence.

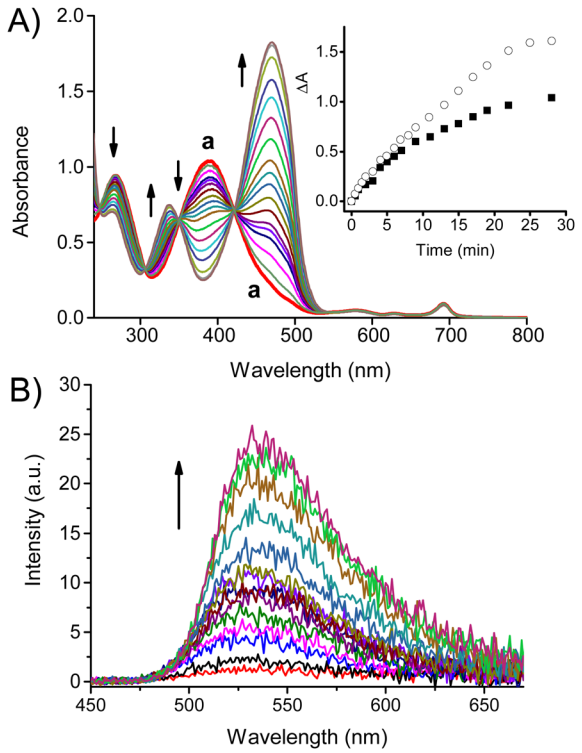

Fig. 2 (A) Absorption spectral changes observed upon exposure of an N_2-saturated aqueous dispersion of PLMs (1% w/v) co-encapsulating **NBF-NO** (60 μM) and **VTP** (1.5 μM) at λ_{ac} = 630 nm (*ca.* 30 mW cm^{-2}) for time intervals from 0 (spectrum a) to 28 min. The arrows indicate the course of the spectral profile with the illumination time. The inset shows the difference absorbance changes at λ = 470 nm observed in N_2-saturated (○) and air-equilibrated (■) conditions as a function of the irradiation time. (B) Evolution of the fluorescence emission spectra corresponding to the sample of Fig. 2A and recorded at λ_{exc} = 420 nm (isosbestic point). T = 25 °C.

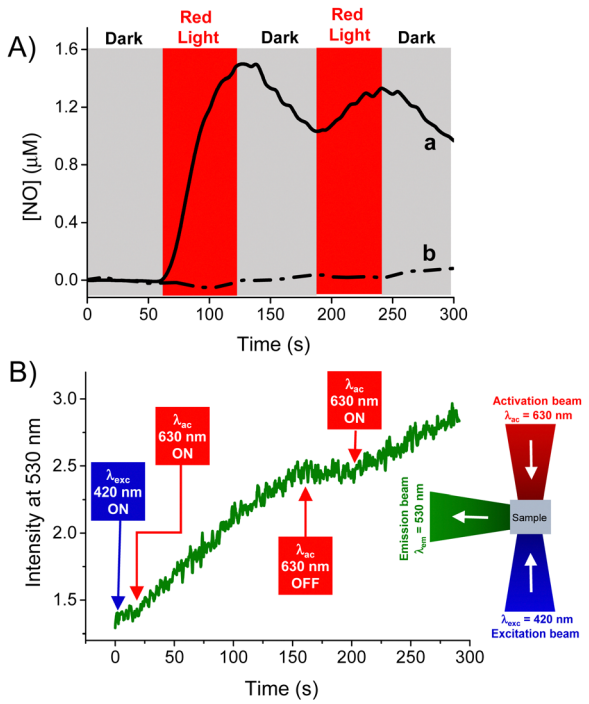

Fig. 3 (A) NO release profiles observed for an air-equilibrated aqueous dispersion of PLMs (1% w/v) co-encapsulating **NBF-NO** (60 μM) and **VTP** (1.5 μM) (a) and, as control, only **VTP** (b) upon alternate cycles of red-light irradiation at λ_{ac} = 671 nm. T = 25 °C. (B) Real-time fluorescence intensity monitored at λ_{em} = 530 nm and observed in an air-equilibrated dispersion of PLMs (1% w/v) co-encapsulating **NBF-NO** (60 μM) and **VTP** (1.5 μM) keeping constant the excitation source at λ_{exc} = 420 nm and alternating ON/OFF cycles of the red light activation source at λ_{ac} = 630 nm. The schematic of the optical experimental set-up used is also shown.

release. These experimental conditions permit the PSs to be selectively activated with red light at $\lambda_{ac} > 600$ nm.

To promote the communication between PSs and **NBF-NO**, these molecules were loaded in three biocompatible host vehicles that share biocompatibility and excellent optical transparency. The latter property represents an ideal requisite for spectroscopic and photochemical investigations. PLMs are supramolecular structures with a hydrophobic core of polypropylene oxide able to encapsulate hydrophobic molecules and a surrounding shell of polyoxyethylene. Micelles prepared using a mixture of Pluronic® F127 and P123 are less inclined to dissociation in monomers upon dilution in aqueous media due to a lower critical micelle concentration (CMC) than the single components.[30]

PLMs were prepared with 1% (w/v) of P123 : F127 at 1 : 1 ratio by wt. Under these conditions, the CMC is 0.0030%, ensuring the formation of micelles with a diameter of *ca.* 30 nm.

The water-insoluble **NBF-NO** was co-encapsulated with the water-insoluble **VTP** at a molar ratio of *ca.* 40 : 1, leading to a nanoassembly of *ca.* 34 nm with a polydispersity index (PI) of 0.18. The UV-Vis absorption profile of this sample (spectrum a in Fig. 2A) matches well the arithmetic sum of the spectra of the individual components encapsulated in the same host (data not shown), accounting for the absence of relevant intra/inter chromophoric aggregation.

Fig. 2A shows the absorption spectral changes observed upon red light irradiation of the sample under anaerobic conditions. They show the bleaching of the absorption bands at 390 nm and 270 nm, and the formation of a new, intense absorption at *ca.* 470 nm accompanied by the presence of 4 isosbestic points, indicative of a well-defined photochemical process. Besides, only negligible spectral changes are observed in the Q band absorption region of **VTP** beyond 550 nm. The corresponding evolution of the fluorescence emission spectra recorded at λ_{exc} = 420 nm (isosbestic point) shows a remarkable increase in the initially weak green emission at λ_{max} = 530 nm (Fig. 2B). The absorption and emission changes observed are in excellent agreement with those reported upon direct irradiation of **NBF-NO** with blue light[27] and are consistent with the formation of the highly green fluorescent NBF as a stable photoproduct. These results parallel those recently observed for the same chromophoric components co-encapsulated within mPEG-PCL NPs,[26] demonstrating that the same photosensitization process also occurs in PLMs. The red-light triggered photosensitization also occurs in the presence of oxygen but at a reduced transformation rate (see the inset in Fig. 2A). This confirms (i) the involvement of the lowest triplet state of **VTP** as a key intermediate in the photosensitization

 This journal is © The Royal Society of Chemistry 2024

Open Access Article. Published on 28 May 2024. Downloaded on 11/8/2025 11:26:02 AM.
This article is licensed under a Creative Commons Attribution 3.0 Unported Licence.

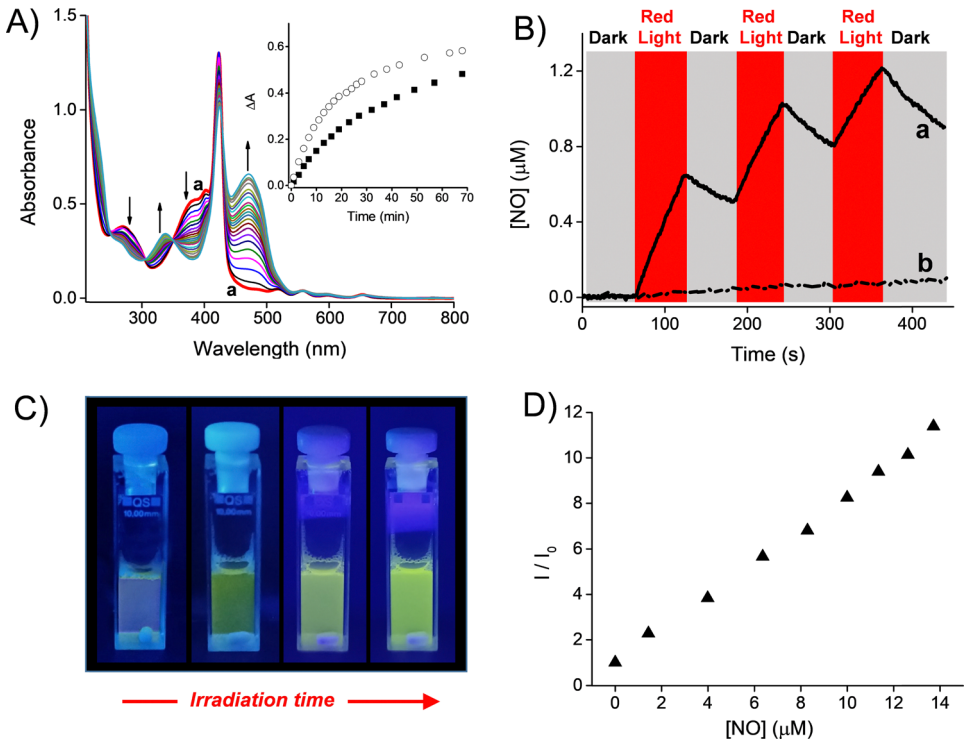

Fig. 4 (A) Absorption spectral changes observed upon exposure of an N_2-saturated aqueous dispersion of PLMs (1% w/v) co-encapsulating **NBF-NO** (30 μM) and **THP** (2 μM) at λ_{ac} = 630 nm (*ca.* 30 mW cm^{-2}) for time intervals from 0 (spectrum a) to 68 min. The arrows indicate the course of the spectral profile with the illumination time. The inset shows the difference absorbance changes at λ = 470 nm observed in N_2-saturated (○) and air-equilibrated (■) conditions as a function of the irradiation time. (B) NO release profiles in air-equilibrated aqueous dispersions of PLMs (1% w/v) co-encapsulating **NBF-NO** (30 μM) and **THP** (2 μM) (a) and, as control, only **THP** (b) upon alternate cycles of red-light irradiation at λ_{ac} = 671 nm. (C) Actual images of the sample as in (A) under illumination with a blue LED and different times of irradiation at λ_{ac} = 630 nm from 0 (left) to 60 min (right). (D) Correlation of the fluorescence increase at λ_{em} = 530 nm (λ_{exc} = 420 nm) observed upon red-light irradiation at λ_{ac} = 671 nm of sample as in (A) under aerobic conditions and the concentration of NO photoreleased measured by direct amperometric detection. I and I_0 represent the fluorescence intensities after and before irradiation, respectively. T = 25 °C.

process and (ii) a quenching by **NBF-NO** highly competitive with that by molecular oxygen.

Unambiguous evidence for the red-light-triggered NO release was provided by its direct detection through an amperometric technique using an ultrasensitive NO electrode. Fig. 3A shows that NO generation exclusively regulated by red light is observed only in the PLM co-loaded with **VTP** and **NBF-NO**.

As already anticipated, the highly fluorescent photoproduct NBF can act as an NO optical reporter, permitting the NO release to be monitored in real-time and exploiting fluorescence techniques. This feature was demonstrated by the experimental set-up illustrated in Fig. 3B. The sample was continuously excited at λ_{exc} = 420 nm, and the fluorescence signal was constantly monitored at λ_{em} = 530 nm upon alternated OFF and ON activation cycles of irradiation with red light at λ_{ac} = 630 nm. It can be seen that the green fluorescence of NBF regularly increases upon irradiation with red light, stops as this light source is turned OFF, and restarts when it is turned ON again. Note that, despite **NBF-NO** absorption at λ_{exc} = 420 nm, the light intensity used in this experiment is not high enough to trigger the NO photorelease by direct photolysis. Although the concentration of **VTP** was 40-fold lower than that of **NBF-NO**, the latter is transformed almost quantitatively into NBF upon red light irradiation. This finding highlights another remarkable point of this strategy: the photocatalytic nature of the photosensitization process. The negligible spectral changes observed in the absorption region of **VTP** beyond 600 nm (see Fig. 2A) suggest only a minor consumption of this PS, in excellent agreement with the photocatalytic mechanism.

Analogously to **VTP**, the NO release was also photosensitized by the red-light irradiation of **THP**, another porphyrinic PS known to generate its low and long-lived triplet state upon light irradiation.[31] **THP** is water insoluble but becomes well soluble under its photoresponsive monomeric form within PLMs. Co-encapsulation of **NBF-NO** leads to supramolecular assemblies with a hydrodynamic diameter of *ca.* 32 nm and a PI of 0.18. The spectroscopic and photochemical results obtained are illustrated in Fig. 4.

Also in this case, the absorption profile of this ternary nanoassembly (spectrum a in Fig. 4A) matches well with the arithmetic sum of the spectra of the individual encapsulated components, accounting for negligible intra/inter chromophoric aggregation. The absorption spectral changes observed upon red light irradiation of the sample under anaerobic conditions are characterized by well-defined isosbestic points, indicating a clean photochemical transformation as in the **NBF-**

Open Access Article. Published on 28 May 2024. Downloaded on 11/8/2025 11:26:02 AM.
This article is licensed under a Creative Commons Attribution 3.0 Unported Licence.

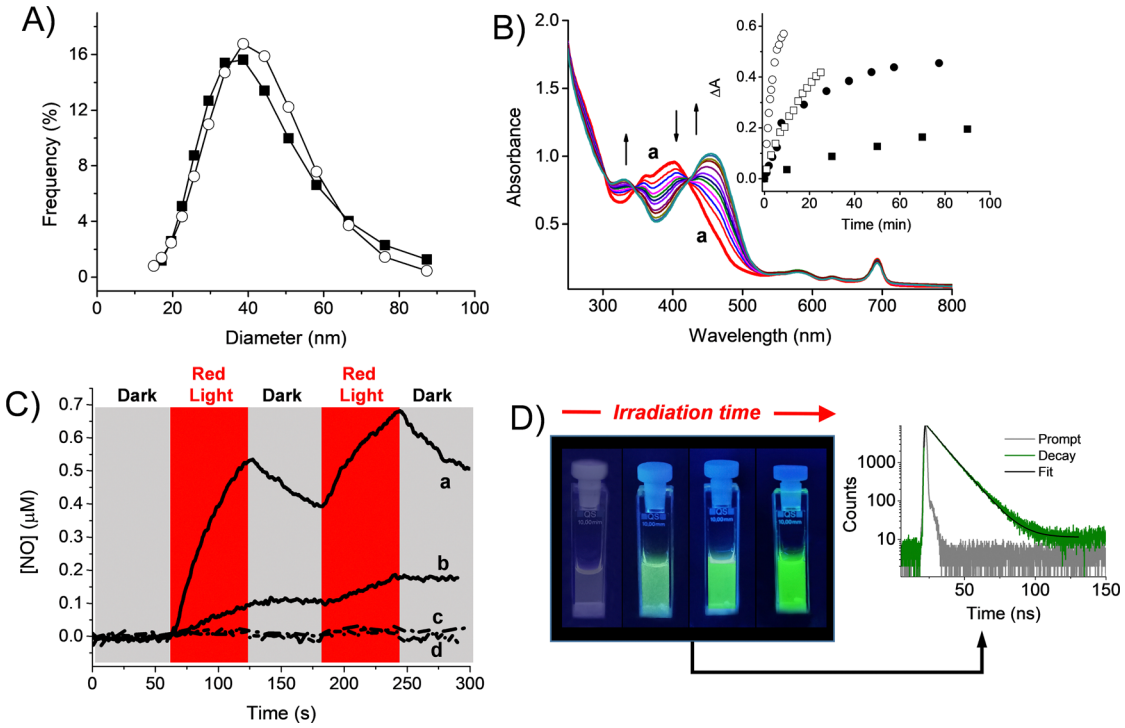

Fig. 5 (A) Hydrodynamic diameters of MEs co-loaded with (○) **NBF-NO** (45 μM) and **VTP** (3 μM) or (■) **NBF-NO** (45 μM) and **THP** (4 μM). (B) Absorption spectral changes observed upon exposure of N_2-saturated MEs co-encapsulating **NBF-NO** (45 μM) and **VTP** (3 μM) at λ_{ac} = 630 nm (*ca.* 30 mW cm^{-2}) for time intervals from 0 (spectrum a) to 9 min. The arrows indicate the course of the spectral profile with the illumination time. The inset shows the difference absorbance changes at λ = 470 nm observed for N_2-saturated (open symbols) and air-equilibrated (solid symbols) MEs co-loaded with **NBF-NO** (45 μM) and **VTP** (3 μM) (circles) and MEs co-loaded with **NBF-NO** (45 μM) and **THP** (4 μM) (square) as a function of the irradiation time. (C) NO release profiles observed for air-equilibrated MEs co-loaded with (a) **NBF-NO** and **VTP** or (b) **NBF-NO** and **THP** and, for sake of control, only **VTP** (c) and **THP** (d), upon alternate cycles of red light irradiation at λ_{ac} = 671 nm. Same concentrations as in (B). (D) Representative actual images of the sample as in (B) acquired under illumination with a blue LED and different times of irradiation at λ_{ac} = 630 nm from 0 (left) to 10 min (right) and representative fluorescence decay and the related fitting recorded at the end of the irradiation and monitored at λ_{exc} = 455 nm and λ_{exc} = 530 nm. T = 25 °C.

NO/VTP case. The absorption profiles show the bleaching of the absorption bands in the 390 and 280 nm region and the simultaneous formation of the intense absorption band at *ca.* 470 nm, typical for the stable photoproduct NBF. The presence of oxygen did not affect the nature of the photolytic process, but slightly affected the phototransformation rate due to the quenching of the **THP** triplet state (see the inset in Fig. 4A). Fig. 4B shows the direct evidence of photosensitized NO release from the nanoassembly, which strictly depends on the presence of the red light irradiation. The emission of the optical reporter NBF is visible even to the naked eye (Fig. 4C) and gives easily readable information about the NO generated. A representative result regarding the role of NBF as a NO reporter is shown in Fig. 4D. The increase in green fluorescence emission is related to the amount of photoreleased NO, measured by its direct detection. Analogously to what was already found using **VTP** as a PS, **NBF-NO** is transformed almost quantitatively into NBF upon red light irradiation of **THP** despite the concentration of this PS being *ca.* 15 fold smaller, in excellent agreement with the photocatalytic nature of the photosensitization process.

The feasibility of the photosensitized NO release from **NBF-NO** by the hydrophobic **VTP** and **THP** was then tested in MEs as an example of a biocompatible nanocarrier with features different from PLMs. MEs are single-phase, optically isotropic nanocarriers made of oil, water, and surfactants with sizes below 100 nm and high thermodynamic stability. In recent years, MEs have gained increasing attention in the pharmaceutical field due to their capability to solubilize and deliver highly lipophilic compounds that remain mainly confined in the apolar phase.[32] MEs tested here are made of Labrafac™ Lipophile WL 1349 and Kolliphor™ HS15, two lipophilic components that are able to solubilize poorly water-soluble molecules. MEs are spontaneously formed under low mixing rates from the Labrafac™ Lipophile WL 1349/Kolliphor HS15 mixture and water in appropriate ratios (see the Experimental section).

NBF-NO is well soluble in MEs, and its co-encapsulation with either **VTP** or **THP** leads to nanoassemblies with similar diameters of *ca.* 33 and 31 nm, respectively, and a PI of *ca.* 0.11 (Fig. 5A). The results obtained with both red-absorbing PSs were very similar to those already found with PLMs and some representative data are summarized in Fig. 5B–D. Fig. 5B shows the absorption spectral changes observed in the case of **NBF-NO** co-encapsulated with **VTP**. The spectral evolution confirms the formation of the NBF as the sole stable photoproduct with its absorption maximum at *ca.* 470 nm. Besides, negligible spectral modifications were observed in the region of the Q band of **VTP** beyond 500 nm, according to the photocatalytic

Open Access Article. Published on 28 May 2024. Downloaded on 11/8/2025 11:26:02 AM.
This article is licensed under a Creative Commons Attribution 3.0 Unported Licence.

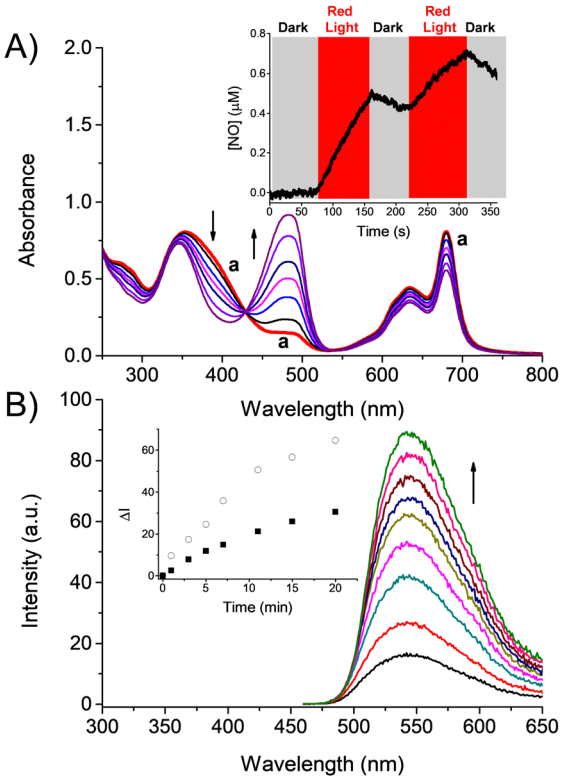

Fig. 6 (A) Absorption spectral changes observed upon exposure of an N_2-saturated aqueous dispersion of poly-βCD (2 mg mL^{-1}) co-encapsulating **NBF-NO** (30 μM) and **ZnPCS** (5 μM of monomer) at λ_{ac} = 671 nm for time intervals from 0 (spectrum a) to 15 min. The arrows indicate the course of the spectral profile with the illumination time. The inset shows NO release profile observed for an air-equilibrated poly-βCD aqueous dispersion as above upon alternate cycles of red light irradiation at λ_{ac} = 671 nm. (B) Evolution of the fluorescence emission spectra corresponding to the sample of Fig. 6A and recorded at λ_{exc} = 420 nm. The inset shows the difference intensity changes at λ_{em} = 530 nm observed in N_2-saturated (○) and air-equilibrated (■) conditions as a function of the irradiation time. T = 25 °C.

photosensitization process. A similar spectroscopic scenario was observed for **THP** (data not shown). As reported in the inset of Fig. 5B, the photochemical transformation sensitized by both **VTP** and **THP** was only in part quenched by molecular oxygen and the NO release under aerobic conditions and red-light irradiation was again confirmed by its direct monitoring (Fig. 5C). Finally, as reported in Fig. 5D, the green emission of the NBF was very intense and visible to the naked eye also in this nanocarrier, and its fluorescence decay was a clean mono-exponential with a lifetime of *ca.* 10 ns (see Fig. 5D). These findings confirm the capability of NBF to act as a NO fluorescent reporter also in MEs.

The validity of the photosensitization strategy to trigger NO release with hydrophilic PSs absorbing red light was finally tested with poly-βCD, a class of branched polymeric nanocarriers made of βCD units crosslinked through the epichlorohydrin crosslinker agent.[33,34] Due to nanodomains with different sizes and polarity, these polymers exhibit high water solubility and can solubilize and stabilize a wide range of guests much more effectively than monomeric βCDs.[33,34] Poly-βCD was appropriately chosen due to its capability to encapsulate hydrophilic compounds besides hydrophobic ones.[35–38] This allows us to extend our strategy also to a PS with hydrophilic features such as **ZnPCS** (see Scheme 1). It is a well-known water-soluble PS for PDT, which exhibits an absorption band in the red region at 635 nm (spectrum e in Fig. 1). However, under these conditions, **ZnPCS** is self-aggregated and non-responsive to light,[39–41] resulting in the ineffective population of its lowest triplet state, which is the indispensable intermediate for the photosensitization mechanism. As already demonstrated in our previous works, poly-βCD significantly breaks the self-aggregation of **ZnPCS**,[35–37] encouraging the entangling within the polymeric network as a photoresponsive monomeric form in a satisfactory amount.

Co-encapsulation of **NBF-NO** and **ZnPCS** within a suspension of poly-βCD leads to a nanoassembly *ca.* 25 nm in diameter. Its absorption spectrum (spectrum a in Fig. 6A) clearly shows a new absorption band with λ_{max} = 680 nm, typical of the monomeric species of **ZnPCS**.[39] Based on the absorbance of this band and the molar absorptivity of the monomeric form, a monomerization degree of *ca.* 30% can be estimated. According to the literature, entrapment of the monomeric **ZnPCS** can be favoured by the 3D structure of the branched polymer in which the high local concentration of the βCD nanocavities in the crosslinked network may act cooperatively in the disruption of the aggregate forms.[42] Irradiation of this ternary complex with red light led, also in this case, to the unambiguous formation of the NBF characterized by the formation of its characteristic absorption at 470 nm and the simultaneous release of NO (inset in Fig. 6A). The green, fluorescence properties of NO were also preserved in this nanocarrier as demonstrated by the remarkable increase in the fluorescence emission upon red light irradiation (Fig. 6B). The absorption and spectral evolution did not change in the presence of oxygen but, analogously to the previous systems, the photoreaction rate was partially slowed down, according to the triplet-mediated photosensitization (inset in Fig. 6B).

An essential point of this work that deserves to be discussed further is the effect of oxygen on the efficiency of NO photorelease. As illustrated above, in all systems investigated, the photo-transformation rate of **NBF-NO** generating NO is in part slowed down by molecular oxygen. This is reasonable since oxygen is a typical triplet quencher. Usually, this diffusional-controlled collisional process leads to the formation of singlet oxygen ($^1O_2$), the key species for PDT.[28] The most suitable method to detect $^1O_2$ is monitoring its typical and very diagnostic phosphorescence in the near-IR spectral window, which exhibits a maximum at 1270 nm.[43] As reported in Fig. 7, $^1O_2$ is photogenerated by all PSs when individually encapsulated in the nanocarriers. In contrast, negligible amounts of $^1O_2$ are observed when the PSs are co-encapsulated with **NBF-NO**. These findings demonstrate that, under the adopted experimental conditions, **NBF-NO** is a highly competitive quencher with molecular oxygen, permitting the photosensitized NO release to occur even under aerobic conditions, although at a slightly slower rate. This competitive quenching by **NBF-NO** can

Open Access Article. Published on 28 May 2024. Downloaded on 11/8/2025 11:26:02 AM.
This article is licensed under a Creative Commons Attribution 3.0 Unported Licence.

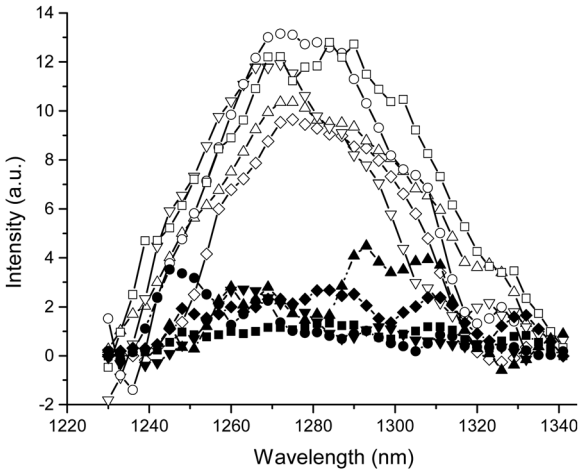

Fig. 7 $^1O_2$ luminescence detected upon 671 nm light excitation of D_2O aqueous dispersions of: (i) PLMs loaded with **VTP** without (○) and with (●) **NBF-NO** and **THP** without (□) and with (■) **NBF-NO**; (ii) MEs loaded with **VTP** without (▽) and with (▼) **NBF-NO** and **THP** without (△) and with (▲) **NBF-NO**; (iii) poly-βCD loaded with **ZnPCS** without (◊) and with (♦) **NBF-NO**. T = 25 °C. The concentration of the PS and the NOPD are the same to those reported in the experiments reported above.

be the result of two opposite effects that are: (i) an increase in the rate constant for the donor/acceptor pairs (PS/NOPD) confined in a restricted space like the host nanoenvironment, typically due to the high local concentration of the reactants;[44] and (ii) a reduction of the quenching constant of the triplet state by the molecular oxygen typically attributable to a shielding effect by host nanocarriers from the external environment.[45,46]

Conclusions

This work demonstrates the validity of a supramolecular strategy to trigger NO release from an otherwise blue-light activatable NOPD with the much more biocompatible and highly tissue-penetrating red light. This occurs through a supramolecular photosensitization process mediated by the lowest triplet state of different PSs co-encapsulated with the NOPD in different biocompatible carrier systems and leads to an improvement of about 300 nm towards a longer excitation wavelength. The process occurs catalytically both under anaerobic and aerobic conditions. It is always accompanied by the formation of a highly green, fluorescent stable photoproduct, which acts as an optical reporter to detect NO release in real-time. A remarkable point of this work is that the proposed strategy does not require any chemical modification efforts on the NOPD used or any excitation with sophisticated two-photon irradiation sources. Studies addressed to bio-applications of the systems presented herein will be performed in our laboratories in the future.

Experimental section

Materials

Pluronic® P123 (EO20–PO70–EO20, MW 5750 g mol^{-1}), Pluronic® F127 (EO100–PO70–EO100, MW 12 600 g mol^{-1}), Kolliphor™ HS15 (Macrogol 15 hydroxystearate), **VTP**, **THP** and **ZnPCS** were purchased from Merck KGaA (Germany). Labrafac™ Lipophile WL 1349, which consists of medium-chain triglycerides of caprylic (C8) and capric (C10) acids, was a kind gift from Gattefossé (France). Poly-βCD (MW *ca.* 100 kDa) was purchased at CycloLab R&D Laboratory, Hungary. **NBF-NO** and **NBF** were synthesized using our already-reported procedures.[27] All other chemicals were purchased by Sigma-Aldrich and used as received. Deionized ultrafiltered water was used throughout this study.

Samples preparation

Polymeric micelles (PLMs). Empty micelles were prepared using the thin-film hydration method.[30] Briefly, 40 mg of Pluronic® (20 mg of P123 and 20 mg of F127) were dissolved in absolute ethanol (4 mL) in a round-bottom flask. Then, the solvent was evaporated by rotary evaporation (35 °C, 25 min) to obtain a film. The film was left under vacuum overnight to remove residual solvent. After that, the dried film was hydrated with 4 mL of water, and the material was sonicated (10 min) giving a micellar solution. The PSs were added by employing the thin-film method: briefly, an ethanolic stock solution was evaporated and stirred with the micelles overnight. Then, *ca.* 1 mg of **NBF-NO** was added to the previously prepared micelles. The sample was stirred for 4 h at room temperature and filtered (0.22 μm filters, RC Chemtek, Italy) to remove the unincorporated components or possible large cylindrical aggregates formed by P123. The actual concentration of the loaded molecules was optimized by dilution with the solution of empty micelles and determined by UV-Vis spectrophotometry.

Microemulsions (ME). An aliquot of **NBF-NO** and PS stock solutions in THF were mixed in appropriate ratios, dried and then dissolved in 0.25 mL of Labrafac™ Lipophile WL 1349 under stirring. Thereafter, 0.5 mL of Kolliphor™ HS 15, previously warmed at 40 °C, were added to the previous solution and stirred for 10 minutes. Thereafter, 4.25 mL of water was added, and the sample was cooled down to room temperature and left to stir (600 rpm) for 30 minutes. The optically transparent resulting MEs were stabilized overnight in the fridge.

Poly-βCDis spectrophotometry.

Poly-βCD (2 mg mL^{-1}) was added to an aqueous solution of the PS. The resulting solution was stirred for 24 h. Then, *ca.* 1 mg of **NBF-NO** was added and left to stir for 4 h in the dark. The actual concentration of the loaded molecules was optimized by dilution with the solution of empty poly-βCD and determined by UV-Vis spectrophotometry.

Instrumentations

UV-Vis spectra absorption and fluorescence emission spectra were recorded with a Perkin Elmer spectrophotometer (mod. Lambda 365) and a Spex Fluorolog-2 (mod. F-111) spectrofluorimeter, respectively, using either quartz cells with a path length of 1 cm. Fluorescence lifetimes were recorded with the same fluorimeter equipped with a TCSPC Triple Illuminator. The samples were irradiated by a pulsed diode excitation source Nanoled at 455 nm. The kinetics was monitored at 540 and the

 This journal is © The Royal Society of Chemistry 2024

Open Access Article. Published on 28 May 2024. Downloaded on 11/8/2025 11:26:02 AM. This article is licensed under a Creative Commons Attribution 3.0 Unported Licence.

solvent was used to register the prompt at 455 nm. The system allowed measurement of fluorescence lifetimes from 200 ps. The exponential fit of the fluorescence decay was obtained using eqn (1):

$$I(t) = \sum \alpha_i \exp(^{-t/\tau_i}) \quad (1)$$

Steady-state irradiation experiments were performed in a thermostated quartz cell (1 cm pathlength, 3 mL capacity) under gentle stirring using an LED source at λ = 630 nm. The photolysis experiments under anaerobic conditions were performed by deoxygenating the solution by bubbling with a vigorous and constant flux of pure nitrogen (previously saturated with solvent).

Direct monitoring of NO release for samples in solution was performed by amperometric detection with a World Precision Instrument, ISO-NO meter, equipped with a data acquisition system, and based on direct amperometric detection of NO with short response time (<5 s) and sensitivity range 1 nM–20 μM. The analog signal was digitalized with a four-channel recording system and transferred to a PC. The sensor was accurately calibrated by mixing standard solutions of $NaNO_2$ with 0.1 M H_2SO_4 and 0.1 M KI according to reaction (2):

$$4H^+ + 2I^- + 2NO_2^- \rightarrow 2H_2O + 2NO + I_2 \quad (2)$$

Irradiation was performed in a thermostated quartz cell (1 cm pathlength, 3 mL capacity) using a continuum red laser at λ_{exc} = 671 nm (100 mW) having a beam diameter of *ca.* 1.5 mm.

NO measurements were carried out under stirring with the electrode positioned outside the light path to avoid NO signal artifacts due to photoelectric interference at the ISO-NO electrode.

The NIR luminescence of $^1O_2$ at 1.27 μm results from the forbidden transition $^3\Sigma_g^- \leftarrow {}^1\Delta_g$. This steady-state emission was registered with the same spectrofluorimeter as above equipped with a NIR-sensitive liquid nitrogen-cooled photomultiplier, exciting the air-equilibrated samples with the above continuum laser with λ_{exc} = 671 nm (200 mW). $^1O_2$ emission was registered in the D_2O solution.

Hydrodynamic diameter (DH), polydispersity index (PdI), and zeta potential (ζ) of the NPs were determined using a Zetasizer Nano ZS (Malvern Instruments Ltd, Malvern, UK). Measurements were performed at a temperature of 25 °C.

Conflicts of interest

There are no conflicts to declare.

Acknowledgements

This research was funded by the European Union – NextGenerationEU through the Italian Ministry of University and Research under PNRR – M4C2-I1.3 Project PE_00000019 ''HEAL ITALIA'' and PNRR-M4C2-I1.1 – MUR Call for proposals no. by PNRR-M4C2-I1.1 – 1409 of 14-09-2022 – PRIN 2022 PNRR – ERC sector PE4-Project title: a molecular platform for intracellular nitric oxide sensing – Project Code P2022F4WR8-CUP Code D53D23016840001.

Notes and references

1 L. J. Ignarro, *Arch. Pharmacal Res.*, 2009, **32**, 1099–1101.
2 L. J. Ignarro, *Nitric Oxide: Biology and Pathobiology*, Elsevier, 2010.
3 A. W. Carpenter and M. H. Schoenfisch, *Chem. Soc. Rev.*, 2012, **41**, 3742–3752.
4 W. Wang, W. Mo, Z. Hang, Y. Huang, H. Yi, Z. Sun and A. Lei, *ACS Nano*, 2023, **17**, 19581–19599.
5 D. Fukumura, S. Kashiwagi and R. K. Jain, *Nat. Rev. Cancer*, 2006, **6**, 521–534.
6 L. Yang, E. S. Feura, M. J. R. Ahonen and M. H. Schoenfisch, *Adv. Healthcare Mater.*, 2018, **7**, 1800155.
7 G. R. Navale, S. Singh and K. Ghosh, *Coord. Chem. Rev.*, 2023, **481**, 215052.
8 D. A. Riccio and M. H. Schoenfisch, *Chem. Soc. Rev.*, 2012, **41**, 3731–3741.
9 A. B. Seabra and N. Durán, *J. Mater. Chem.*, 2010, **20**, 1624–1637.
10 P. G. Wang, T. B. Cai and N. Taniguchi, *Nitric oxide donors: for pharmaceutical and biological applications*, John Wiley & Sons, 2005.
11 P. G. Wang, M. Xian, X. Tang, X. Wu, Z. Wen, T. Cai and A. J. Janczuk, *Chem. Rev.*, 2002, **102**, 1091–1134.
12 Y. Qian, R. Kumar, M. K. Chug, H. Massoumi and E. J. Brisbois, *ACS Appl. Mater. Interfaces*, 2021, **13**, 52250–52273.
13 Z. Huang, J. Fu and Y. Zhang, *J. Med. Chem.*, 2017, **60**, 7617–7635.
14 A. J. Janczuk, Q. Jia, M. Xian, Z. Wen, P. G. Wang and T. Cai, *Expert Opin. Ther. Pat.*, 2002, **12**, 819–826.
15 P. C. Ford, *Nitric oxide*, 2013, **34**, 56–64.
16 P. C. Ford, *Coord. Chem. Rev.*, 2018, **376**, 548–564.
17 A. Fraix, C. Parisi, M. Seggio and S. Sortino, *Chem. – Eur J.*, 2021, **27**, 12714–12725.
18 N. L. Fry and P. K. Mascharak, *Acc. Chem. Res.*, 2011, **44**, 289–298.
19 N. Ieda, Y. Oka, T. Yoshihara, S. Tobita, T. Sasamori, M. Kawaguchi and H. Nakagawa, *Sci. Rep.*, 2019, **9**, 1430.
20 S. Sortino, *Chem. Soc. Rev.*, 2010, **39**, 2903–2913.
21 R. Weissleder, *Nat. Biotechnol.*, 2001, **19**, 316–317.
22 N. Ieda, Y. Hotta, A. Yamauchi, A. Nishikawa, T. Sasamori, D. Saitoh, M. Kawaguchi, K. Kimura and H. Nakagawa, *ACS Chem. Biol.*, 2020, **15**, 2958–2965.
23 C. Parisi, M. Failla, A. Fraix, L. Menilli, F. Moret, E. Reddi, B. Rolando, F. Spyrakis, L. Lazzarato, R. Fruttero, A. Gasco and S. Sortino, *Chem. Sci.*, 2021, **12**, 4740–4746.
24 X. Bao, S. Zheng, L. Zhang, A. Shen, G. Zhang, S. Liu and J. Hu, *Angew. Chem., Int. Ed.*, 2022, **61**, e202207250.
25 X. Zhang, J. Du, Z. Guo, J. Yu, Q. Gao, W. Yin, S. Zhu, Z. Gu and Y. Zhao, *Adv. Sci.*, 2019, **6**, 1801122.
26 A. Fraix, C. Parisi, G. Longobardi, C. Conte, A. Pastore, M. Stornaiuolo, A. C. E. Graziano, M. E. Alberto,

Open Access Article. Published on 28 May 2024. Downloaded on 11/8/2025 11:26:02 AM.
This article is licensed under a Creative Commons Attribution 3.0 Unported Licence.

A. Francés-Monerris, F. Quaglia and S. Sortino, *Biomacromolecules*, 2023, **24**, 3887–3897.
27 C. Parisi, M. Seggio, A. Fraix and S. Sortino, *ChemPhotoChem*, 2020, **4**, 742–748.
28 J. P. Celli, B. Q. Spring, I. Rizvi, C. L. Evans, K. S. Samkoe, S. Verma, B. W. Pogue and T. Hasan, *Chem. Rev.*, 2010, **110**, 2795–2838.
29 M. T. Huggett, M. Jermyn, A. Gillams, R. Illing, S. Mosse, M. Novelli, E. Kent, S. G. Bown, T. Hasan, B. W. Pogue and S. P. Pereira, *Br. J. Cancer*, 2014, **110**, 1698–1704.
30 X. Zhang, J. K. Jackson and H. M. Burt, *Int. J. Pharm.*, 1996, **132**, 195–206.
31 A. C. M. Montalti, L. Prodi and M. T. Gandolfi, *Handbook of Photochemistry*, 3rd edn, CRC, Boca Raton, 2006.
32 A. Fraix, O. Catanzano, I. Di Bari, C. Conte, M. Seggio, C. Parisi, A. Nostro, G. Ginestra, F. Quaglia and S. Sortino, *J. Mater. Chem. B*, 2019, **7**, 5257–5264.
33 M. Agnes, E. Pancani, M. Malanga, E. Fenyvesi and I. Manet, *Macromol. Biosci.*, 2022, **22**, e2200090.
34 M. Othman, K. Bouchemal, P. Couvreur, D. Desmaële, E. Morvan, T. Pouget and R. Gref, *J. Colloid Interface Sci.*, 2011, **354**, 517–527.
35 A. Fraix, N. Kandoth, I. Manet, V. Cardile, A. C. E. Graziano, R. Gref and S. Sortino, *Chem. Commun.*, 2013, **49**, 4459–4461.
36 A. Fraix, V. Kirejev, M. Malanga, É. Fenyvesi, S. Béni, M. B. Ericson and S. Sortino, *Chemistry*, 2019, **25**, 7091–7095.
37 N. Kandoth, V. Kirejev, S. Monti, R. Gref, M. B. Ericson and S. Sortino, *Biomacromolecules*, 2014, **15**, 1768–1776.
38 M. Malanga, M. Seggio, V. Kirejev, A. Fraix, I. Di Bari, E. Fenyvesi, M. B. Ericson and S. Sortino, *Biomater. Sci.*, 2019, **7**, 2272–2276.
39 L. Howe and J. Zhang, *J. Phys. Chem. A*, 1997, **101**, 3207–3213.
40 M. Morisue, S. Ueda, M. Kurasawa, M. Naito and Y. Kuroda, *J. Phys. Chem. A*, 2012, **116**, 5139–5144.
41 A. Ogunsipe, J.-Y. Chen and T. Nyokong, *New J. Chem.*, 2004, **28**, 822–827.
42 B. Brożek-Płuska, A. Jarota, K. Kurczewski and H. Abramczyk, *J. Mol. Struct.*, 2009, **924–926**, 338–346.
43 P. R. Ogilby, *Chem. Soc. Rev.*, 2010, **39**, 3181–3209.
44 G. Rothenberger, P. P. Infelta and M. Graetzel, *J. Phys. Chem.*, 1979, **83**, 1871–1876.
45 S. Monti and S. Sortino, *Chem. Soc. Rev.*, 2002, **31** 287–300.
46 C. Parisi, G. Longobardi, A. C. E. Graziano, A. Fraix, C. Conte, F. Quaglia and S. Sortino, *Bioorg. Chem.*, 2022, **128**, 106050.

 This journal is © The Royal Society of Chemistry 2024